Article:
Ismail, M.S., Mohamed, A.M., Poggio, D. et al. (2021) Direct contact membrane distillation : a sensitivity analysis and an outlook on membrane effective thermal conductivity. Journal of Membrane Science, 624. 119035. ISSN: 0376-7388

https://doi.org/10.1016/j.memsci.2020.119035

Direct contact membrane distillation: a sensitivity analysis and an outlook on membrane effective thermal conductivity

M.S. Ismail [a, b *], A.M. Mohamed [c], D. Poggio [a], M. Pourkashanian [a, b]

[a] Energy 2050, Department of Mechanical Engineering, University of Sheffield, Sheffield S3 7RD, United Kingdom.

[b] Translational Energy Research Centre (TERC), University of Sheffield, Sheffield S3 7RD, United Kingdom

[c] Faculty of Engineering, Port Said University, Port Said, Port Foad 42526, Egypt

[*] Corresponding author: Tel: +44 114 21 57242

Email addresses: m.s.ismail@sheffield.ac.uk, msaeedaaal@gmail.com (M.S. Ismail)

Abstract

A rigorous and high-fidelity two-dimensional numerical model for a direct contact membrane distillation (DCMD) module has been developed. The developed model incorporates all the key physics governing the transport phenomena taking place within the membrane distillation (MD) module. The spatial variation of the physical properties of the fluids flowing in the channels and the membrane with temperature has been captured. The model has been used to investigate the sensitivity of the key performance indicators or KPIs (i.e. the transmembrane flux, the thermal efficiency and the temperature polarisation coefficient) to ten key operational conditions and membrane characteristics. The models used to estimate the effective thermal conductivity of the membranes have been discussed and it was shown that more appropriate models are required to accurately estimate the latter parameter and, to this end, a new model has been proposed.

Keywords: Direct contact membrane distillation; Numerical model; Key performance indicators; Sensitivity analysis; Membrane effective thermal conductivity

1. Introduction

Membrane distillation (MD) is a thermally-driven distillation method used in desalination, wastewater treatment, food processing, biomedical applications and many other applications [1-2]. Compared to other membrane separations (e.g. reverse osmosis), MD has multiple advantages: (i) almost perfect rejection of non-volatile solutes (e.g. salt), (ii) substantially larger pore size, (iii) less sensitivity to fouling, (iv) less vulnerability to feed salinity and (v) possible use of low-grade heat or renewable energy [3-4]. Direct contact membrane distillation (DCMD) is a form of the MD in which both heated liquid feed and cold liquid permeate are in direct contact with a porous hydrophobic membrane, and a temperature difference between the two streams causes a vapour pressure difference across the membrane that drives a transmembrane flux [5]. There are, depending upon the nature of the cold side of the MD module, three more common configurations [6]: (i) vacuum membrane distillation (VDM) where the vapour phase is vacuumed from the liquid through the membrane and is, if needed, condensed externally (e.g. [7]), (ii) air gap membrane distillation (AGMD) where an air gap is placed between the membrane and a condensation surface (e.g. [8]) and (iii) sweeping gas membrane distillation (SGMD) where an inert gas is used to sweep the produced vapour which is, if needed, condensed externally (e.g. [9]). Compared to other configurations, the design of DCMD is simple [1]: (i) it does not require an air gap or a condensation plate (as is the case in AGMD), (ii) it requires no external condensers (as is the case for VMD or SGMD), vacuum pumps (as is the case for VMD) or gas compressors (as is the case for SGMD).

Numerical modelling is an efficient and cost-effective way to provide insights on the effects of the operational conditions and the design parameters on the performance of the membrane distillation modules. The transmembrane flux of water vapour is typically the most commonly-used key performance indicator (KPI) of the MD modules. There are two more KPIs that are often reported in the literature: the thermal efficiency (η_t) and the temperature polarisation

coefficient (TPC); all of the above KPIs will be defined and discussed in Section 3. Surprisingly, there have been only few numerical models to simulate the operation of the DCMDs despite the relative simplicity of the physics describing the transport phenomena taking place within the DCMD module. The below is a brief account of the key findings of the numerical DCMD models that have been encountered while performing the literature survey.

Park et al. [1] developed a two-dimensional model to investigate each of the following parameter on the transmembrane flux: the operating conditions, the salinity of the feed stream, the flow configuration (counter-flow versus co-flow), the insertion of the mesh screen (used to mechanically support the membrane) and the spacing between the filaments of the mesh screen. They found that the insertion of the mesh screen, in particular that with small spacing between its filaments, improves the transmembrane flux of the modelled module and this is due to the improved hydrodynamics of the flow (increased velocities and mixing) around the filaments. Likewise, Shakib et al. [10] created a two-dimensional model and showed that the TPC is sensitive to the positions of the filaments and how they are arranged in the channels (staggered versus inline). Yu et al. [11] developed a two-dimensional model for a baffled/non-baffled hollow fibre based DCMD module. They found that the transmembrane flux and the TPC in general improve when introducing baffles.

Chen et al. [12] created a two-dimensional model for a plate and frame DCMD module. They employed a finite difference method to linearise the partial differential equations used for the conservation equations of mass, momentum and energy and solved them using the fourth-order Runge-Kutta method. They particularly explored the effect of feed flow rate and temperature on the transmembrane flux. Similarly, there were two-dimensional models developed to investigate the effects of flow configuration and geometrical parameters of the channels [13]; the thermal conductivity of the membrane and the presence of air gap [14] on the KPIs, in particular the transmembrane flux. Isam et al. [15] developed a two-dimensional model and

proposed optimal values for the operating conditions and the membrane thermal conductivity for a DCMD equipped with a flat sheet PVFD membrane. Perfilov et al. [16] found that, using a two-dimensional model they developed, the transmembrane flux substantially increases with increasing inlet feed temperature. Hayer et al. [17] created a two-dimensional model and studied the effects of five parameters (i.e. feed and permeate flow rates, inlet feed temperature, membrane thickness and salinity). They conducted a sensitivity analysis and found that, for the given ranges they considered, the salinity has almost no effect on the transmembrane flux and the TPC. Rezakazemi [18] developed a two-dimensional model and explored the effects of the inlet flow rates and the inlet feed temperature on the outlet temperatures of the feed and permeate channels.

In all the above modelling investigations, there have been no clear and well-defined frameworks with which the sensitivity of the KPIs of the distillation module to the operational conditions and the design parameters could be satisfactorily realised; it is often that only one KPI is considered, few parameters are investigated and/or the characteristics of the membrane are overlooked. Further, there have been no agreement on which model to use to calculate the effective thermal conductivity of the modelled distillation membranes despite the significant influence of this parameter on all the KPIs. To this end, a two-dimensional numerical model has been developed to comprehensively investigate for the first time the sensitivity of the KPIs of the DCMD module to ten operational conditions and membrane characteristics. Further, the inaccuracies associated with the commonly-used models to calculate the effective thermal conductivity of the membrane have been discussed and subsequently a new model has been proposed.

2. Model formulation

The geometry considered and modelled in this study is for a DCMD module that was investigated in [12]; all the physical parameters needed to build and run the model were provided in [12] and therefore no fitting parameters and/or assumed values were used in the model. The geometrical parameters, amongst other parameters, are shown in Table 1.

Table 1 Key parameters of the modelled DCMD [12].

Parameter	Value
Channel height	0.002 m
Module length (L)	0.21 m
Membrane porosity (ε)	0.72
Membrane thickness (t_m)	130 µm
Average pore dimeter (d_p)	0.1 µm
Thermal conductivity of membrane material (k_s)	0.178 W m^{-1} K^{-1}
Salinity (w_s)	3.5 wt. %

The flow in the feed and the permeate channels is assumed to be incompressible, steady and laminar and it is therefore governed by the following form of conservation of mass and momentum equations:

$$\rho \nabla . (\boldsymbol{u}) = 0 \tag{1}$$

$$\rho(\boldsymbol{u}.\boldsymbol{\nabla})\boldsymbol{u} = \boldsymbol{\nabla}.(-p\boldsymbol{I} + \mu(\boldsymbol{\nabla u} + (\boldsymbol{\nabla u})^{\boldsymbol{T}})) \tag{2}$$

where $\boldsymbol{u}$ is the velocity vector, ρ and μ are the density and the dynamic viscosity of the flowing fluid and p is the pressure. Note that $\boldsymbol{I}$ is the identity tensor. The transfer of heat is governed by the conservation of energy equation:

$$\rho . C_p . \boldsymbol{u} . \nabla T + \nabla . (-k \nabla T) + S_T = 0 \tag{3}$$

where C_p is the specific heat capacity at a constant pressure (J kg^{-1} K^{-1}), T is the temperature and k is the thermal conductivity which is calculated for the membrane using the following expression:

$$k_{eff} = \varepsilon k_g + (1 - \varepsilon) k_s \quad (4)$$

where k_{eff} is the effective thermal conductivity of the membrane and k_g is the thermal conductivity of the void-filling gas which is water vapour in this case and calculated using the following empirical expression [12]:

$$k_g = 0.0144 - 2.16 \times 10^{-5} T + 1.32 \times 10^{-7} T^2 \quad (5)$$

The solute (e.g. salt) was assumed to have no effect on the properties of liquid water, the flowing fluid in the feed and the permeate channels, and therefore the temperature-dependent polynomials of pure water were used for the thermal conductivity and other properties (i.e. ρ, C_p and μ); see Appendix A. The source term S_T is zero in the channels and equals to the rate of spatial change of the heat of vaporisation in the membrane:

$$S_T = \nabla . (h_{fg} J) \quad (6)$$

where h_{fg} is the latent heat of vaporisation (kJ kg^{-1}) and J is the transmembrane flux of water water (kg m^{-2} s^{-1}). Compared to the existing models, a more rigorous approach was adopted to calculate the above-mentioned source term: (i) the heat of vaporisation was not simply assumed to be constant but to change with temperature following the equation that was fitted using some tabulated data for saturated water vapour [19]: $h_{fg} = -2.4324T + 3167.2$ and subsequently (ii) the local change of the product $h_{fg}J$ was accounted for (it was not simply divided by the thickness of the membrane). The convective term, the first term in Eq. (3), was assumed to be negligible within the pores of the membrane; it was estimated that the heat convection only accounts for less than 1% of the total heat transferred across the membrane [20]. The transmembrane flux of water vapour in the membrane is given by:

$$\nabla . (N) = 0 \quad (7)$$

$$N = -D_{eff} \nabla C_w \quad (8)$$

$$J = N.M_w \tag{9}$$

where N and J are the molar and mass flux of water vapour respectively, M_w is the molecular weight of water (i.e. 0.018 kg mol^{-1}) and D_{eff} is the effective diffusivity of water vapour. For membranes with pores less than 0.5 µm, molecule-pore collisions become as frequent as molecule-molecule collisions and therefore Knudsen diffusion must be taken into account [20]:

$$D_{eff} = \frac{\varepsilon}{\tau}\left[\frac{1}{D_w} + \frac{1}{D_K}\right]^{-1} \tag{10}$$

where ε is the porosity of the membrane and τ is the tortuosity of the membrane which is assumed to follow the Bruggeman correlation (i.e. $\tau = 1/\sqrt{\varepsilon}$) [4]. D_w is the normal diffusion coefficient of water vapour and is given by [21]:

$$D_w = 1.895 \times 10^{-5} \frac{T^{2.072}}{101325} \tag{11}$$

and D_K is the Knudsen diffusion coefficient [22]:

$$D_K = \frac{4d_p}{3}\left(\frac{RT}{2\pi M_w}\right)^{0.5} \tag{12}$$

where d_p is the pore diameter and R is the universal gas constant (8.3145 J mol^{-1} K^{-1}). C_w is the concentration of water vapour and is given by:

$$C_w = a_w x_w \frac{p_s}{RT} \tag{13}$$

where a_w and x_w are the activity coefficient and mole fraction of liquid water which both equal to one at the interface contacting the permeate stream due to 100% purity of water. However, we have a saline solution at the interface between the membrane and the feed stream and therefore the water activity should be taken into account [20]:

$$a_w = 1 - 0.5x_{NaCl} - 10x_{NaCl}^2 \tag{14}$$

where x_{NaCl} is the mole fraction of the chemical NaCl (salt) which was calculated to be 0.011 for 3.5 wt. % NaCl solution. p_s is the saturation pressure of water vapour which could be estimated using Antoine equation [20]:

$$\ln(p_s) = 23.1964 - \frac{3816.44}{T - 46.13} \tag{15}$$

Boundary conditions

Fig. 1 is a schematic of the modelled geometry that shows the boundary conditions used to solve the conservation equations employed in the model. Inlet velocities ($\boldsymbol{u}_{hi}$ and $\boldsymbol{u}_{ci}$) and temperatures (T_{hi} and T_{ci}) are prescribed at the inlets of the channels and zero pressures are prescribed at the outlets of the channels. No slip boundary conditions are imposed at the walls of the channels. Molar concentrations, calculated via Eq. (13), are prescribed at the left (C_{wl}) and the right (C_{wr}) boundaries of the membrane. Where appropriate, no heat flux ($-n.q = 0$) and no molar flux ($-n.N = 0$) are implemented as shown in Fig. 1.

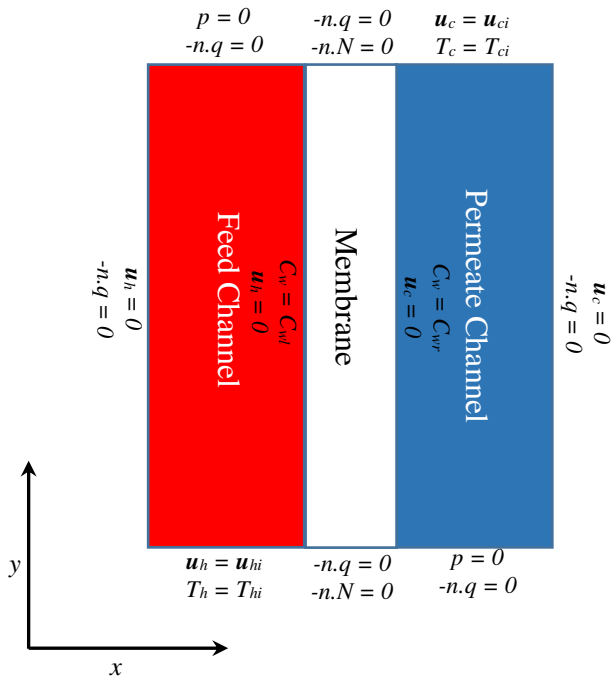

Fig. 1 The boundary conditions used to solve the model. Note that *N* is the molar flux and equal to $-D_{eff}\nabla C_w$ and *q* is heat flux and equal to $-k\nabla T$. The schematic is not to scale.

Meshing and solver

The geometry (comprising of the domains for the feed channel, permeate channel and the membrane) was meshed as shown in Fig. 2. The mesh is structured and is substantially finer at the boundaries and the interfaces of the domains in order to capture the expected high rates of change of the investigated variables in these regions. The number of the elements of the meshed geometry is 9000 which was found to provide a mesh-independent solution. Eq. (1), Eq. (2), Eq. (3) and Eq. (7) were discretised and solved using COMSOL Multiphysics 5.2a® solver.

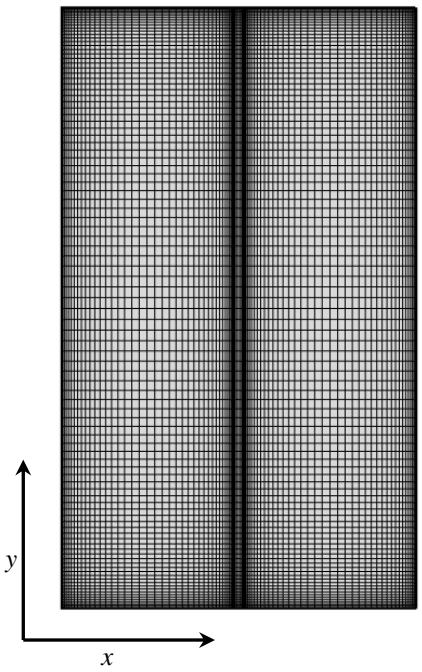

Fig. 2 The meshed computational domain. Note that the dimensions (the height of each channel, 0.002 m, and the membrane thickness, 130 μm) in x-direction are, compared to the length of the module in the y-direction (i.e. 0.21 m), scaled up 30 times in order to present a clearer view of the mesh.

3. Results and discussion

Multiple sets of experimental data from two different sources [12, 13] were used to assess the accuracy of the predictions of the developed model. Fig. 3 shows good agreement between the output of the developed model and experimental data reported in [12] for the transmembrane flux as a function of inlet velocities and feed temperature; the trends are captured and the discrepancies between any two sets of experimental and modelling data are less than 15%. Likewise, a good agreement is obtained between the computed transmembrane flux and the transmembrane flux reported in [13] especially for the case in which the inlet feed temperature is 40 °C (Fig. 4a). Note that the discrepancy between the experimental and predicted data with the high inlet feed velocities and temperature (Fig. 3 and Fig. 4a) is probably due to the positive effect of the turbulence created by high flows set in the experiments in terms of removing the potentially formed bubbles at the surface of the membrane contacting the feed stream; thus reducing the resistance to the transport of water vapour across the membrane. Fig. 4b shows the experimental [13] and the computed outlet temperatures of the feed and permeate channels as they change with inlet velocities; the graph shows a very good agreement between the two sets of data. Note that, as mentioned in Section 2, the geometry of the DCMD module reported in [12] was selected to be modelled in this work and this is due to the availability of all the physical parameters required to build and run the model. The developed model was slightly adapted for the module reported in [13] to account for the changes in the values of some parameters; see the caption of Fig. 4.

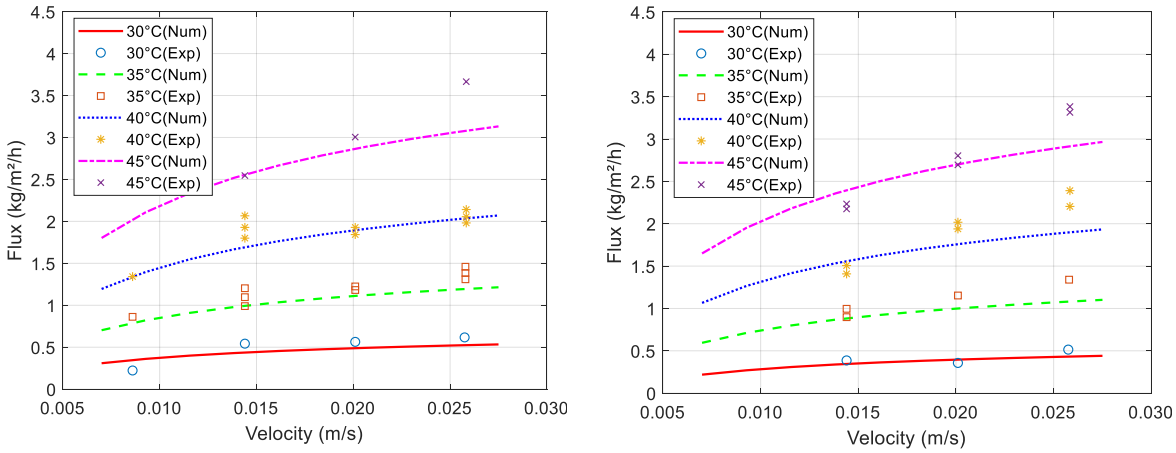

Fig. 3 The transmembrane flux as a function of inlet velocities and feed temperature for: (a) fresh water and (b) saline solution (3.5 wt. % NaCl) as a feed stream. Note that the inlet permeate temperature was kept constant at 20°C and the flow configuration was co-flow [12].

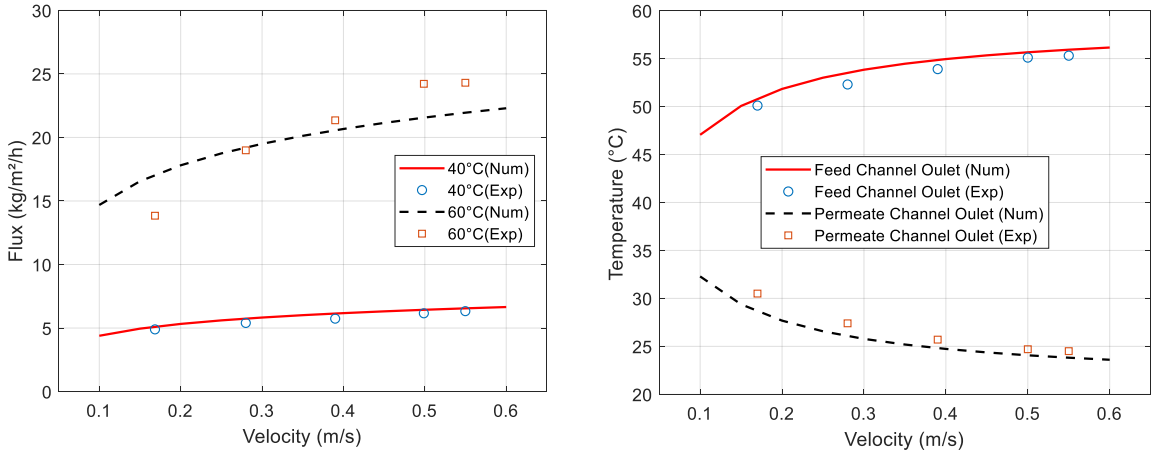

Fig. 4 (a) The transmembrane flux as a function of inlet velocities for two inlet feed temperatures (40 and 60°C) and (b) the outlet temperatures of the feed and permeate channels as they change with inlet velocities. The width and the height of each channel in the module reported in [13] are 1 mm and 0.4 m, respectively. The salinity (w_s), the average pore diameter of the membrane (d_p), the membrane thickness (t_m), the porosity of the membrane (ε) and thermal conductivity of the membrane material k_s used for the respective model are: 1%, 0.28 µm, 100 µm, 0.72 and 0.178 W m^{-1} K^{-1}, respectively.

Base case

In addition to the parameters listed in Table 1, the operating conditions used for the base case are shown in Table 2. The flow configuration considered was, following the normal practice, counter-current. Fig. 5 shows: the contours plot of the velocities in the channels (Fig. 5a); the contour plot of temperature in the entire computational domain (Fig. 5b); and the molar concentration of water vapour in the membrane (Fig. 5c). It is clear that, for the given inlet

velocities, the flow becomes hydrodynamically fully developed after a short distance from the inlets of the channels; almost in less than one fourth of the length of the channel (Fig. 5a). On the other hand, the flow is thermally developing as it is evident from Fig. 5b. Fig. 5c shows that the flux of water vapour is a maximum immediately after the inlet of the feed channel and just before the outlet of the permeate channel; this is because the difference in the concentration of saturated water vapour across the membrane (i.e. the driving force for the transport of water vapour across the membrane) is a maximum in this region where the thickness of the thermal boundary layer is a minimum at the feed channel and subsequently the saturation pressure of water vapour, which increases exponentially with temperature, is a maximum.

Table 2 The values of the variables used for the base case.

Parameter	Value
Inlet velocity of feed stream ($\boldsymbol{u}_{hi}$)	0.2 m s^{-1}
Inlet velocity of permeate stream ($\boldsymbol{u}_{ci}$)	0.2 m s^{-1}
Inlet temperature of feed stream (T_{hi})	60 °C
Inlet temperature of permeate stream (T_{ci})	20 °C

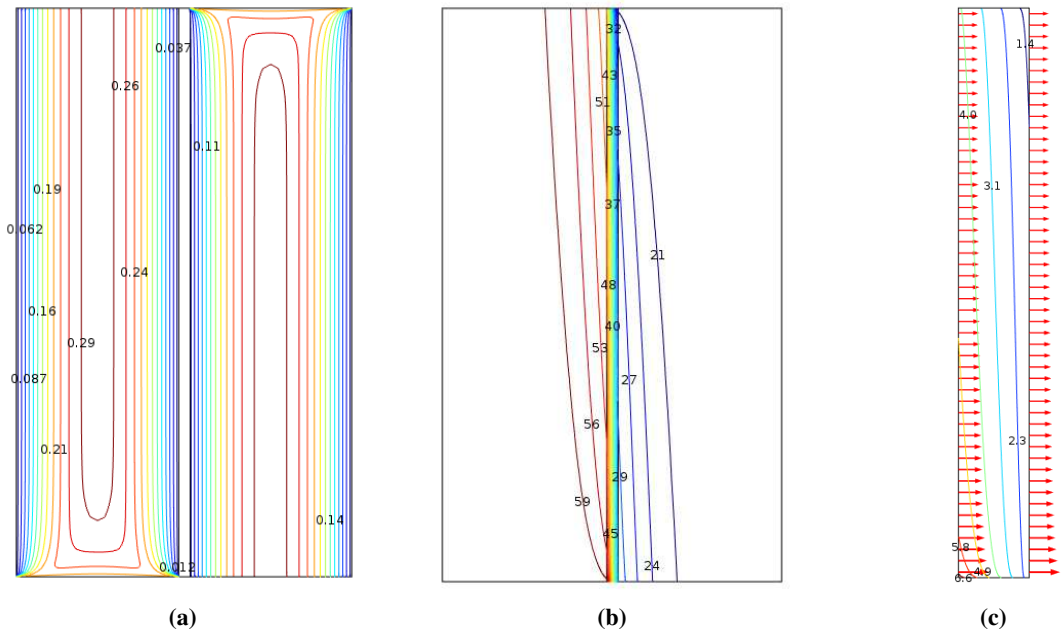

(a) **(b)** **(c)**

Fig. 5 Contour plots of (a) velocity (m s^{-1}), (b) temperature (°C) and (c) concentration of water vapour (mol m^{-3}) in the membrane. Note that the thickness of the membrane domain in (c) was scaled up 200 times and that the red arrows represent the flux of water vapour (mol m^{-2} s^{-1}).

Sensitivity analysis

The value of each parameter used for the base case was, while keeping the values of all other parameters unchanged, varied by ±30% and the KPIs (the transmembrane flux of water vapour ($\bar{J}$), the thermal efficiency (η_t) and the temperature polarisation coefficient (TPC)) were computed for each case.

Table 3 shows the base, maximum and minimum values for each parameter used in the sensitivity analysis.

Table 3 The base, minimum and maximum values of the parameters used in the sensitivity analysis.

Parameter	Base value	Minimum value (-30%)	Maximum value (+30)
Inlet velocity of feed stream ($\boldsymbol{u}_{hi}$)	0.20 m s^{-1}	0.14 m s^{-1}	0.26 m s^{-1}
Inlet velocity of permeate stream ($\boldsymbol{u}_{ci}$)	0.20 m s^{-1}	0.14 m s^{-1}	0.26 m s^{-1}
Inlet temperature of feed stream (T_{hi})	60 °C	42 °C	78 °C
Inlet temperature of permeate stream (T_{ci})	20 °C	14 °C	26 °C
Porosity of membrane (ε)	0.720	0.504	0.936
Tortuosity of membrane (τ)	1.5*	1.05	1.95
Average pore diameter (d_p)	0.10 µm	0.07 µm	0.13 µm
Membrane thickness (t_m)	130 µm	91 µm	169 µm
Thermal conductivity of membrane material (k_s)	0.178 W m^{-1} K^{-1}	0.125 W m^{-1} K^{-1}	0.231 W m^{-1} K^{-1}
Salinity (w_s)	3.50%	2.45%	4.55%

** The original tortuosity value that was used in the base case was 1.18; however, it gives a value less than 1 when reducing it by 30% (the tortuosity cannot be less than 1) and therefore it was changed to 1.5 in this sensitivity analysis.*

($\bar{J}$) is averaged over the length of the membrane:

$$\bar{J} = \frac{1}{L}\int_0^L J\, dy \tag{16}$$

η_t is defined as follows:

$$\eta_t = \frac{q_{l,t}}{q_{l,t} + q_{c,t}} \tag{17}$$

where $q_{l,t}$ is the total heat flux due to phase change and $q_{c,t}$ is the total of heat loss due to conduction through the membrane:

$$q_{l,t} = \int_0^{A_{mem}} q_l \, dA \tag{18}$$

$$q_l = h_{fg}.J \tag{19}$$

$$q_{c,t} = \int_0^{A_{mem}} q_c \, dA \tag{20}$$

$$q_c = -k\nabla.T \tag{21}$$

It is evident that minimising the heat loss due to conduction improves the thermal efficiency of the MD; this could be primarily achieved through the employment of membranes with low thermal conductivities. TPC is defined as:

$$TPC = \frac{\bar{T}_{mf} - \bar{T}_{mp}}{\bar{T}_f - \bar{T}_p} \tag{22}$$

where $\bar{T}_f$ and $\bar{T}_p$ are the temperatures of the feed and permeate streams averaged over the feed and the permeate channels respectively and $\bar{T}_{mf}$ and $\bar{T}_{mp}$ are the temperatures averaged over the interfaces of the membrane with the feed and the permeate channels respectively. TPC is a measure on how effective the exchange of heat is between the streams and the interfaces with the membrane. The higher is the TPC, the lower is the resistance to the transfer of heat from/to the channels to/from the interfaces with the membrane.

Fig. 6 shows the changes of the KPIs with the investigated parameters. Note the exponential relation between $\bar{J}$ and each of the inlet temperature of the feed stream (T_{hi}), the porosity (ε) and the tortuosity (τ) of the membrane signalling that any slight change in the above parameters could have a significant impact on the production of fresh water. Further, $\bar{J}$ appears to ultimately reach asymptotic values with increasing inlet velocities of feed ($\boldsymbol{u}_{hi}$) and permeate ($\boldsymbol{u}_{ci}$) streams implying that a small gain is realised with substantially high velocities (this was confirmed by running the model with substantially high velocities (not shown)). This observation also applies to the average pore dimeter of the membrane (d_p) and this is due to

the diminishing effects of Knudsen diffusion with increasing d_p where molecule-molecule collision (molecular diffusion) dominates.

In order to quantitatively assess the impact of each parameter used in the base case on the KPIs, the gain in the KPI is calculated. The gain is defined herein as the difference between the maximum and minimum values of the KPI, typically obtained at the maximum and the minimum values set for the parameter, divided by the minimum value of the KPI. To illustrate, the gain in the transmembrane flux of water vapour ($\bar{J}$) when changing the base value of the membrane thickness (t_m) by ±30% calculated as follows:

$$Gain_{\bar{J}} = \frac{\bar{J}_{169\mu m} - \bar{J}_{91\mu m}}{\bar{J}_{169\mu m}} 100 = \frac{10.196 - 14.314}{10.196} 100 = -40.39\%$$

The minus sign indicates that the relationship is inversely proportional, meaning that the transmembrane flux of water vapour increases by more than 40% if the membrane thickness decreases from 169 to 91 µm. The same procedure was performed for each parameter. Fig. 7 presents the sensitivity graphs of the KPIs (i.e. $\bar{J}$, η_t and TPC) to the key operational conditions and membrane characteristics; the following observations and comments could be made:

- $\bar{J}$ is highly sensitive to the inlet temperature of the feed stream (T_{hi}); it increases more than 5-fold as the temperature increases from 42 to 78°C. This is due to the exponential increase of saturation pressure of water vapour with temperature as it is evident from Eq. (15). The sensitivity of $\bar{J}$ to the inlet temperature of the permeate stream (T_{ci}) is substantially less than T_{hi} as the relationship between the temperature and saturation pressure of water vapour in the respective range (i.e. 14 – 26 °C) is more linear. To this end, if the source of the thermal energy coupled with the DCMD module is not of financial concern (e.g. industrial waste heat), then it is recommended to fully utilise the heat source to maximise T_{hi}.

- Apart from T_{hi}, the characteristics of the membrane have in general substantially greater effects on the modelled MD module than the operational conditions. Notably, the porosity of the membrane (ε) has, amongst other characteristics of the membrane, the largest impact on the KPIs. Namely, increasing ε from ~ 0.50 to ~ 0.94 results in a 3-fold increase in $\bar{J}$, 2-fold increase in η_t and around 50% increase in the TPC. As ε increases, the diffusion rate of water vapour across the membrane increases. Further, the increase in ε decreases the effective thermal conductivity of the membrane, thus resulting in less heat loss through the conduction and ultimately higher η_t and TPC. By contrast, the tortuosity of the membrane (τ) has an opposite effect on all the KPIs. As intuitively expected and as evident from Eq. (10), as τ increases, the diffusion rate of water vapour across the membrane decreases. The increase in the average pore diameter of the membrane (d_p) has a positive effect on the KPIs. If d_p increases, Knudsen diffusion decreases, thus allowing for more water vapour to be transported through normal diffusion across the membrane. $\bar{J}$, due to increased mas transport resistance, decreases with increasing membrane thickness (t_m). On the other hand, TPC increases with increasing t_m owing to the increased resistance to heat transfer through conduction. Notably, η_t vey slightly increases with increasing t_m from 91 to 169 μm. As expected, the KPIs are inversely related to the thermal conductivity of the material of the membrane (k_s). As k_s increases, both η_t and TPC decrease as the heat loss via conduction increases. This indirectly affects $\bar{J}$ as the decrease in the temperature difference across the membrane leads to less difference in the saturation pressure of water vapour between the two sides of the membrane.
- For the given range, salinity of feed stream (w_s) has almost no effect on all the KPIs, signalling that it could be neglected when modelling the DCMD module. Hwang et al. [13] investigated a wider range for salinity and found about 10% decrease in water vapour flux when increasing salinity from 1 to 6%.

- The increased flow rates of the feed ($\boldsymbol{u}_{hi}$) and the permeate ($\boldsymbol{u}_{ci}$) streams enhance the TPC as the thermal boundary layer at either side of the membrane decrease. η_t slightly increases with increasing $\boldsymbol{u}_{hi}$ and slightly decrease with increasing $\boldsymbol{u}_{ci}$ as the temperature difference across the membrane, the driving force for heat conduction, increases as $\boldsymbol{u}_{hi}$ increases and decreases as $\boldsymbol{u}_{ci}$ increases. The effect of $\boldsymbol{u}_{hi}$ and $\boldsymbol{u}_{ci}$ on $\bar{J}$ are similar to that on η_t as the difference in temperature leads to a difference in saturation pressure of water vapour. However, the effect of $\boldsymbol{u}_{hi}$ on $\bar{J}$ is substantially higher than that of $\boldsymbol{u}_{ci}$ and this is due to the exponential relationship between saturation pressure of water vapour and temperature.

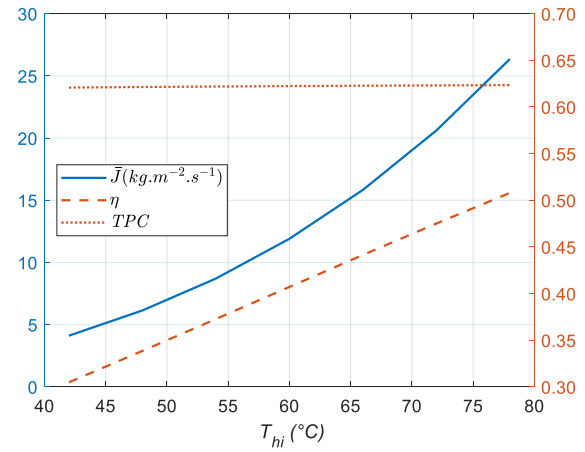

(a)

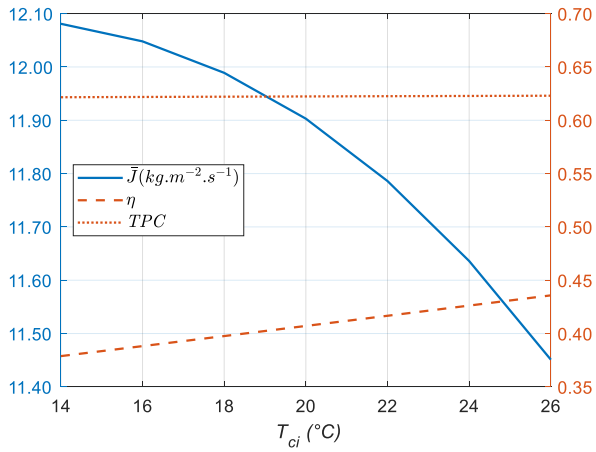

(b)

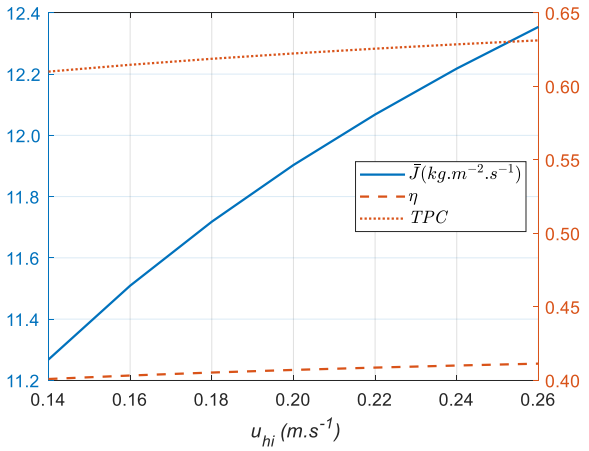

(c)

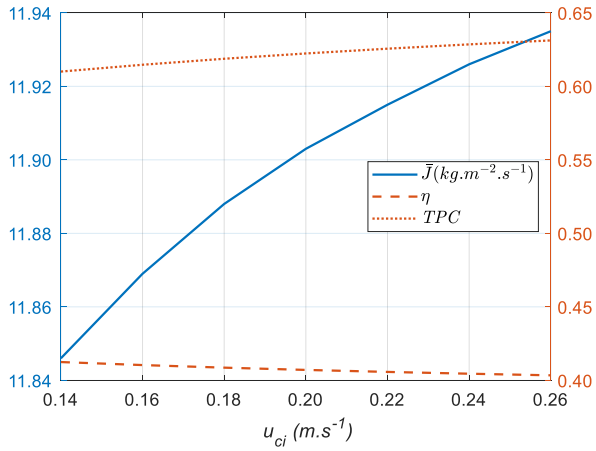

(d)

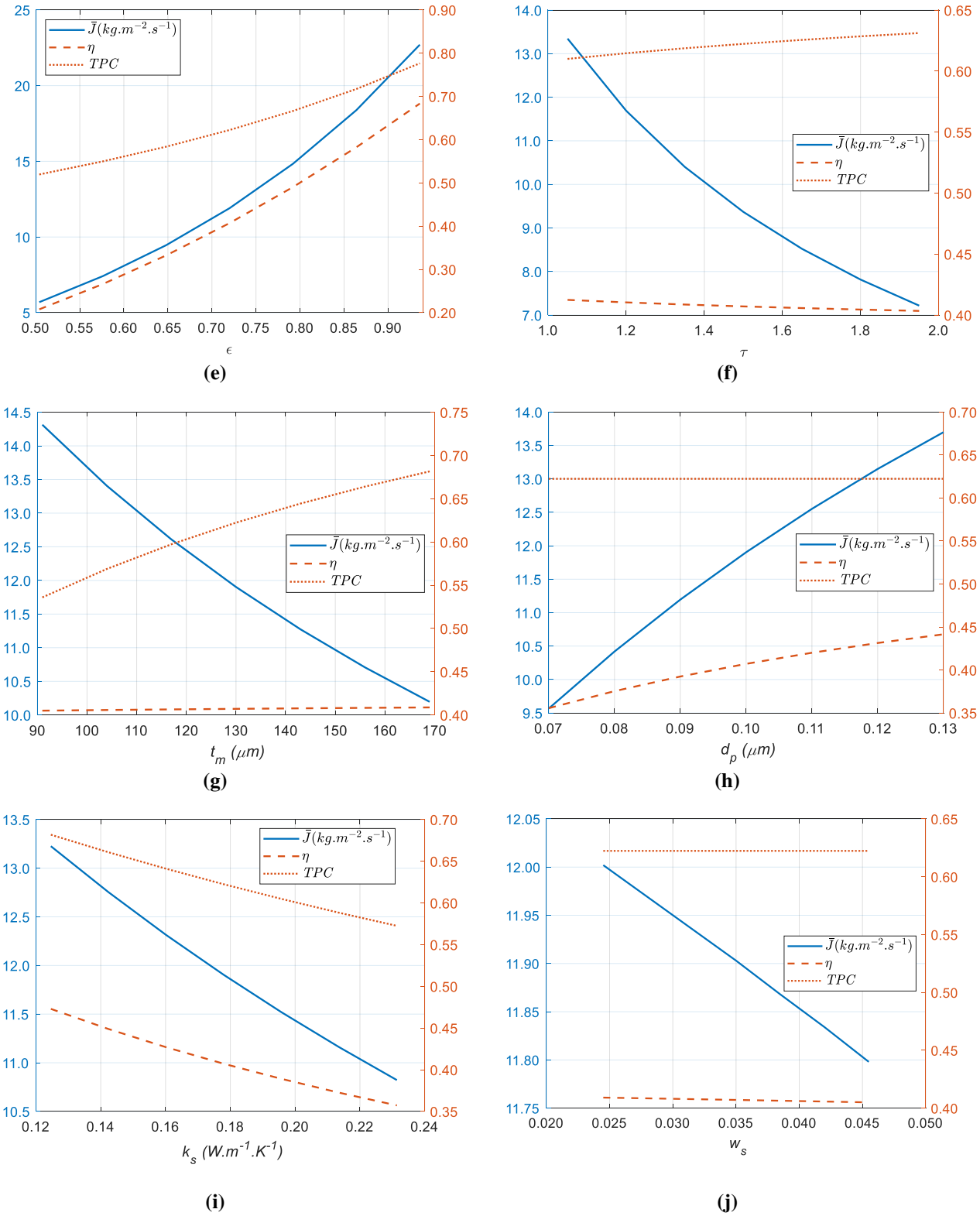

Fig. 6 The transmembrane flux ($\bar{J}$), thermal efficiency (η_t), and temperature polarisation coefficient (TPC) as functions of: (a) inlet feed temperatures (T_{hi}), (b) inlet permeate temperature (T_{ci}), (c) inlet feed velocity (u_{hi}), (d) inlet permeate velocity (u_{ci}), (e) porosity (ε), (f) tortuosity (τ), (g) membrane thickness (t_m), (h) average pore diameter (d_p), (i) thermal conductivity of the solid phase (k_s) and (j) salinity of water (w_s).

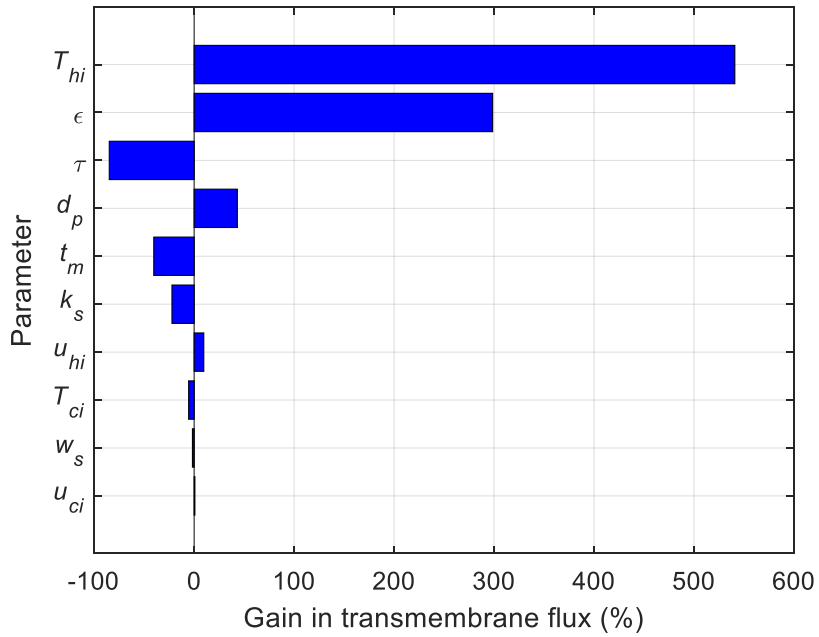
T_{hi}
ϵ
τ
d_p
t_m
k_s
u_{hi}
T_{ci}
w_s
u_{ci}
Parameter
-100
0
100
200
300
400
500
600
Gain in transmembrane flux (%)

(a)

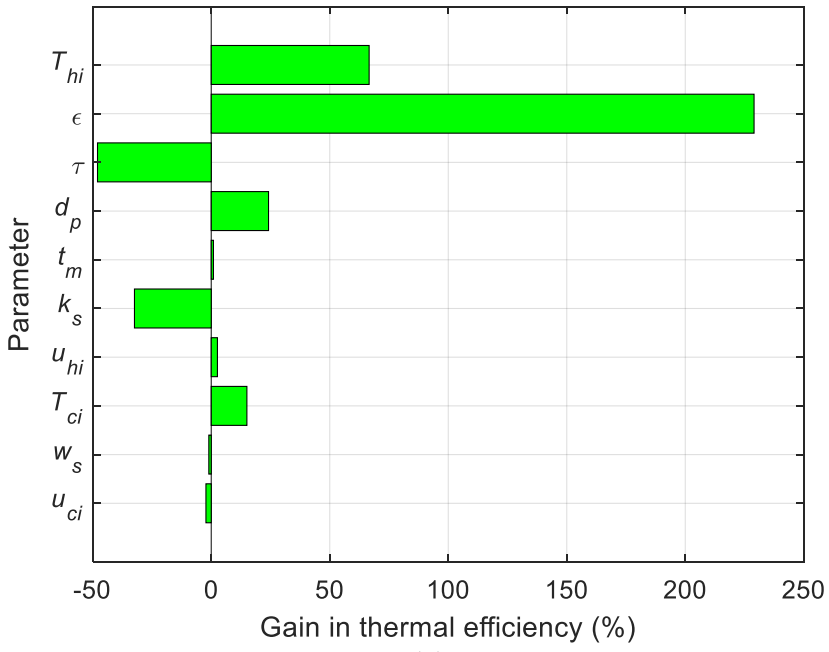
T_{hi}
ϵ
τ
d_p
t_m
k_s
u_{hi}
T_{ci}
w_s
u_{ci}
Parameter
-50
0
50
100
150
200
250
Gain in thermal efficiency (%)

(b)

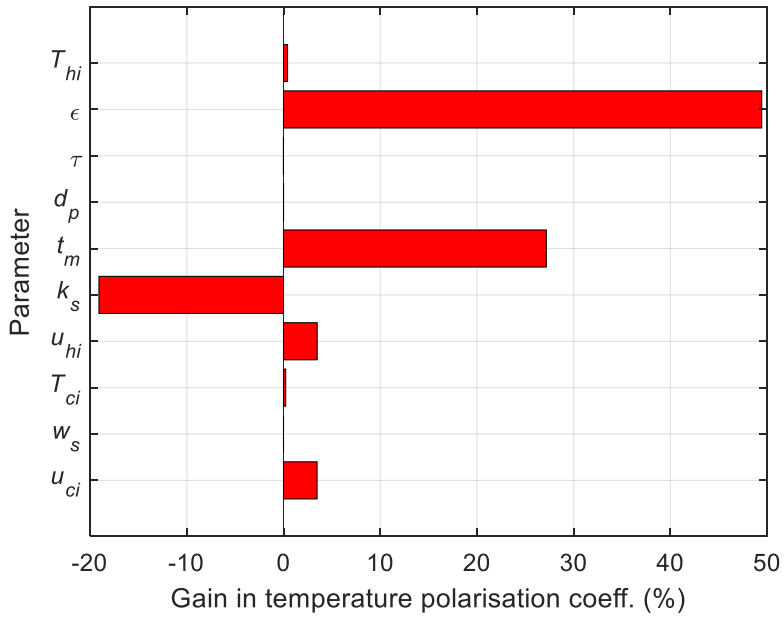

(c)

Fig. 7 Sensitivity of (a) transmembrane flux ($\bar{J}$) (b) thermal efficiency (η_t) and (c) temperature polarisation coefficient (TPC) to the key operational conditions and membrane characteristics: inlet temperatures of the feed and permeate streams (T_{hi} and T_{ci}); inlet velocities of the feed and permeate streams (u_{hi} and u_{ci}); porosity (ε), tortuosity (τ), average pore diameter (d_p), thickness (t_m) and the thermal conductivity of the solid phase (k_s) of the membrane; and salinity of water (x_s).

The sensitivity of the KPIs may change with changing the base values of the investigated parameters. It was shown earlier that the inlet temperature of the feed stream (T_{hi}) has the highest impact on the transmembrane flux of water vapour ($\bar{J}$). T_{hi} is one of the operating conditions that could be, relative to for example the membrane characteristics, easily controlled. To this end, it would be of interest to investigate the sensitivity of the KPIs (in particular $\bar{J}$) to the investigated parameters when changing the base value of T_{hi} from a typically used one (60 °C) [1, 20, 22] to a lower (40°C) or a higher value (80°C). Table 4 and Fig. 8 present the sensitivity of the KPIs to the investigated parameters at three different base values for T_{hi}: 40, 60 and 80 °C (Table 4 was provided to allow for reading of some gain values that could not be easily read from the bar charts shown in Fig. 8). To keep the main body of the paper less cluttered with too many graphs, the changes of the KPIs with the investigated parameters for the base T_{hi} of 40 and 80 °C are moved to Fig. A1and Fig. A2 in Appendix B.

In general, the sensitivity trends of the KPIs with T_{hi} of 40 and 80 °C remain more or less the same as those with 60 °C. However, there are some few distinct trends that need to be highlighted and described:

- $\bar{J}$ and η_t are in general more sensitive to the characteristics of the membrane (ε, τ, t_m and k_s) at low T_{hi} (40 °C); the temperature at the interface between the membrane and the feed channel with such a low T_{hi} is relatively small, creating, compared to higher values of T_{hi}, less driving force (i.e. the difference in saturation pressure of water vapour) for the transport of water vapour across the membrane. This allows for the characteristics of the membrane to play a more profound role in facilitating the transport of water vapour across the two sides of the membrane.
- The gain in $\bar{J}$ with increasing T_{hi} with a base value of 80 °C is more than that with 60 °C base value and this is evidently due to exponential relation between the saturation pressure of water vapour and temperature. Notably, $\bar{J}$ is more sensitive to T_{hi} with a base value of 40 °C than that with 60 °C base value; this is attributed due to the sharp switch from the rather linear region to the start of the exponential region within the investigated range associated with 40 °C T_{hi} (i.e. 28 - 42 °C).
- $\bar{J}$ and η_t are more sensitive to the inlet velocity of the feed stream ($\boldsymbol{u}_{hi}$) with high T_{hi} as the increased thermal conductivity of liquid water with temperature conducts more heat from the feed stream to the interface between the feed channel and the membrane, thus increasing the temperature of the latter and subsequently increasing the gradient of saturation pressure of water vapour across the membrane.
- Fig. A2 (d) and Table 4 shows that $\bar{J}$ decreases with increasing inlet velocity of permeate stream ($\boldsymbol{u}_{ci}$) with high T_{hi} (80 °C); however, $\bar{J}$, with intermediate (60 °C) or low (40 °C) T_{hi}, increases with increasing $\boldsymbol{u}_{ci}$. As $\boldsymbol{u}_{ci}$ increases, more heat is driven away from the module, lowering the temperature of the interface separating the membrane and the

permeate channel and, to a lesser extent, the temperature of the interface separating the membrane and the feed channel. To this end, the rate of decrease of the temperature of the interface between the membrane and the feed channel increases with increasing $\boldsymbol{u}_{ci}$ at high T_{hi} (80 °C), resulting in a decreasing gradient of saturation pressure of water vapour across the membrane.

- The results show that, with low (40 °C) and intermediate (60 °C) T_{hi}, $\bar{J}$ decreases with increasing inlet temperature of permeate stream (T_{ci}); however, with high T_{hi} (80 °C), $\bar{J}$ appears to increase with increasing T_{ci}. As T_{ci} increases, heat transfer rate from the feed side evidently decreases, thus increasing the temperature of the interface between the membrane and the permeate channel and, to a lesser extent, the temperature of the interface between the membrane and the feed channel. Considering the exponential relationship between the saturation pressure of water vapour and temperature, with a T_{hi} of 80 °C, the increase of the temperature of the interface between the membrane and the feed channel is sufficiently high to maintain $\bar{J}$ increasing with increasing T_{ci}. If T_{ci} is (with a T_{hi} of 80 °C) further increased beyond the upper bound of the investigated range (14 – 26 °C), $\bar{J}$ starts to decrease with increasing T_{ci} as the increase in the temperature of the interface between the membrane and the feed channel (and the resulting saturation pressure of water vapour at this temperature) is not sufficiently high to outweigh the larger increase in the temperature of the interface between the membrane and the permeate channel (and the resulting saturation pressure of water vapour at this temperature); see Fig. 9.
- $\bar{J}$ and η_t are more sensitive to salinity with low T_{hi} (40 °C) as the saturation pressure of water vapour at the membrane-feed channel interface is relatively small; therefore, water activity (defined by Eq. (14)), relative to the situation with higher T_{hi} (e.g. 80 °C), has a more profound effect in reducing the gradient of saturation pressure of water vapour across the membrane.

Table 4 The gain in the KPIs as the investigated parameters change for three different inlet feed temperature (T_{hi}): 40, 60 and 80 °C.

	T_{hi} (°C)								
	40			60			80		
	$\bar{J}$	η_t	TPC	$\bar{J}$	η_t	TPC	$\bar{J}$	η_t	TPC
Inlet velocity of feed stream (u_{hi})	7.47	1.74	3.49	9.64	2.61	3.48	11.56	2.89	3.54
Inlet velocity of permeate stream (u_{ci})	2.62	-1.45	3.52	0.75	-2.24	3.47	-0.65	-2.40	3.39
Inlet temperature of feed stream (T_{hi})	690	59.36	0.42	541	66.61	0.42	572	70.54	0.37
Inlet temperature of permeate stream (T_{ci})	-41.93	19.85	0.26	-5.50	15.04	0.23	2.31	10.70	0.19
Porosity of membrane (ε)	303.71	318.25	50.36	298.61	229.02	49.45	288.28	161.80	48.64
Tortuosity of membrane (τ)	-85.57	-58.34	0.00	-84.92	-47.99	0.01	-83.34	-37.83	0.02
Average pore diameter (d_p)	42.76	28.94	0.00	43.20	24.17	0.00	42.66	19.14	0.00
Membrane thickness (t_m)	-40.81	0.80	27.32	-40.39	0.92	27.18	-39.26	1.18	27.10
Thermal conductivity of membrane material (k_s)	-22.42	-40.09	-19.32	-22.21	-32.40	19.08	-21.90	-25.32	18.90
Salinity (w_s)	-2.60	-1.83	0.00	-1.73	-1.02	0.00	-1.45	0.69	0.00

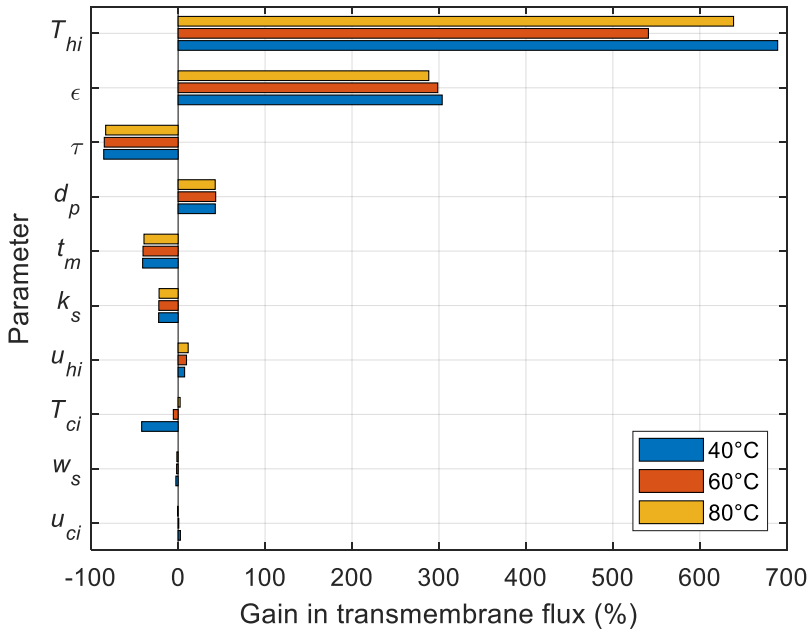
T_{hi}
ϵ
τ
d_p
t_m
k_s
u_{hi}
T_{ci}
w_s
u_{ci}
Parameter
40°C
60°C
80°C
-100
0
100
200
300
400
500
600
700
Gain in transmembrane flux (%)

(a)

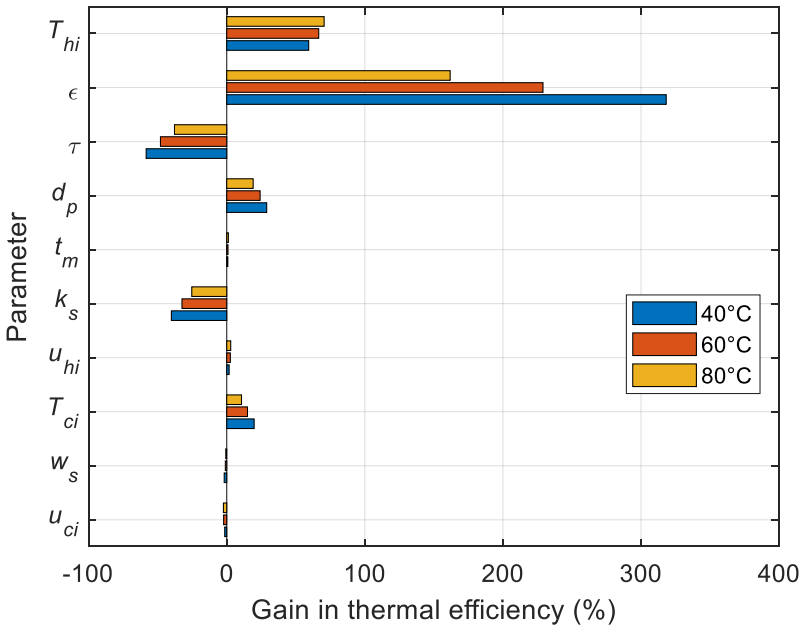
T_{hi}
ϵ
τ
d_p
t_m
k_s
u_{hi}
T_{ci}
w_s
u_{ci}
Parameter
40°C
60°C
80°C
-100
0
100
200
300
400
Gain in thermal efficiency (%)

(b)

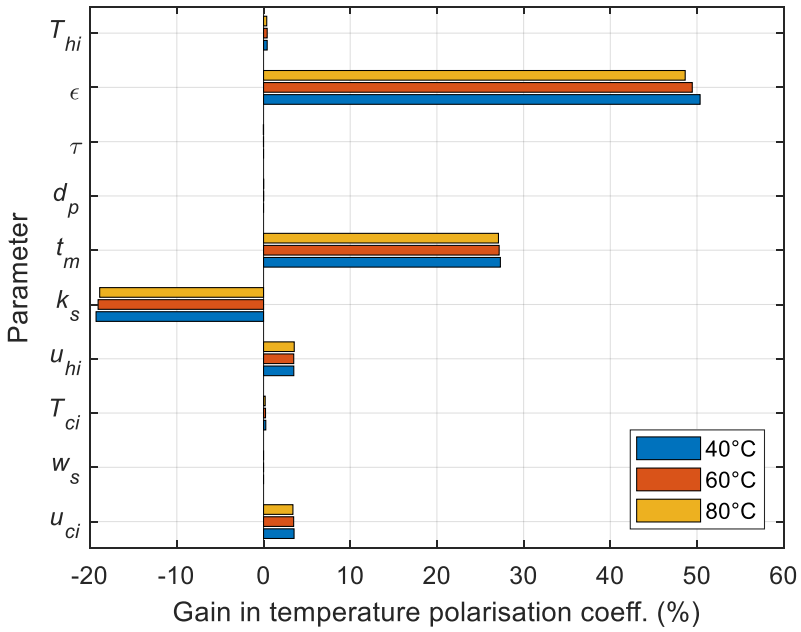

(c)

Fig. 8 Sensitivity of (a) transmembrane flux ($\bar{J}$) (b) thermal efficiency (η_t) and (c) temperature polarisation coefficient (TPC) at low (40° C), intermediate (60°C) and high (80°C) inlet feed temperatures to the key operational conditions and membrane characteristics: inlet temperatures of the feed and permeate streams (T_{hi} and T_{ci}); inlet velocities of the feed and permeate streams (u_{hi} and u_{ci}); porosity (ε), tortuosity (τ), average pore diameter (d_p), thickness (t_m) and the thermal conductivity of the solid phase (k_s) of the membrane; and salinity of water (x_s).

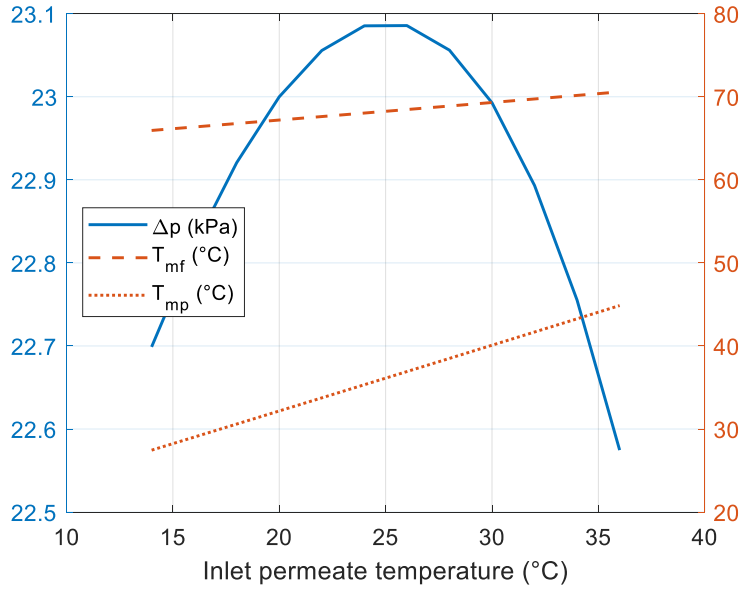

Fig. 9 The average temperatures of the interfaces of the membrane with the feed channel (T_{mf}) and the permeate channel (T_{mf}), and the resulting difference in saturation pressure of water vapour (Δp) as they change with the inlet permeate temperature. The base value of the inlet feed temperature (T_{hi}) is 80 °C.

Thermal conductivity model

As shown in the previous section, the thermal conductivity of the material of the membrane has a significant effect on all the KPIs. The membrane is typically porous and therefore comprises of solid and gaseous phases. The effective thermal conductivity is often calculated using Eq. (4) based on the assumption that the solid and gaseous phases are in parallel configuration (Fig. 10a). On the other hand, there have been few investigations (e.g. [1], [23]) which assumed that the above two phases are in series configuration (Fig. 10b) and therefore the following expression should be used to calculate the effective thermal conductivity of the membrane:

$$k_{eff} = \left[\frac{\varepsilon}{k_g} + \frac{1-\varepsilon}{k_s}\right]^{-1} \tag{23}$$

Notably Phattaranawick et al. [24] suggested that, upon holding a comparison with the measured thermal conductivities of some membranes, the series model is more appropriate than the parallel model for the calculation of the effective thermal conductivity of the membrane. However, they used the thermal conductivity of air to calculate k_{eff}. If they used the thermal conductivity of water vapour, the discrepancy between the calculated and measured k_{eff} will be substantially larger. One could infer from an SEM micrograph for a typical membrane (Fig. 11) that the configuration is neither series nor parallel; it appears to be a combination of the two configurations which could be approximated by the representation shown in Fig. 10c. To this end, the following expression could be proposed to calculate the effective thermal conductivity of distillation membranes:

$$k_{eff} = \alpha\left[\varepsilon k_g + (1-\ \varepsilon)k_s\right] + (1-\alpha)\left[\frac{\varepsilon}{k_g} + \frac{1-\varepsilon}{k_s}\right]^{-1} \tag{24}$$

where α is a weight factor. If α is one, the model is parallel and if it is zero, then the model is series. If it is anything between zero and one, then the model is a combination of the two models (parallel-series model). Table 5 shows the measured thermal conductivity for a number of

distillation membranes and the corresponding calculated thermal conductivity using the expressions for the parallel, series and the parallel-series models. It could be seen that the discrepancy between the measured and the calculated thermal conductivity is in general minimised when using the parallel-series model with an α having a value of around 0.2. This signals that the fibres of the membranes are more oriented in the lateral directions.

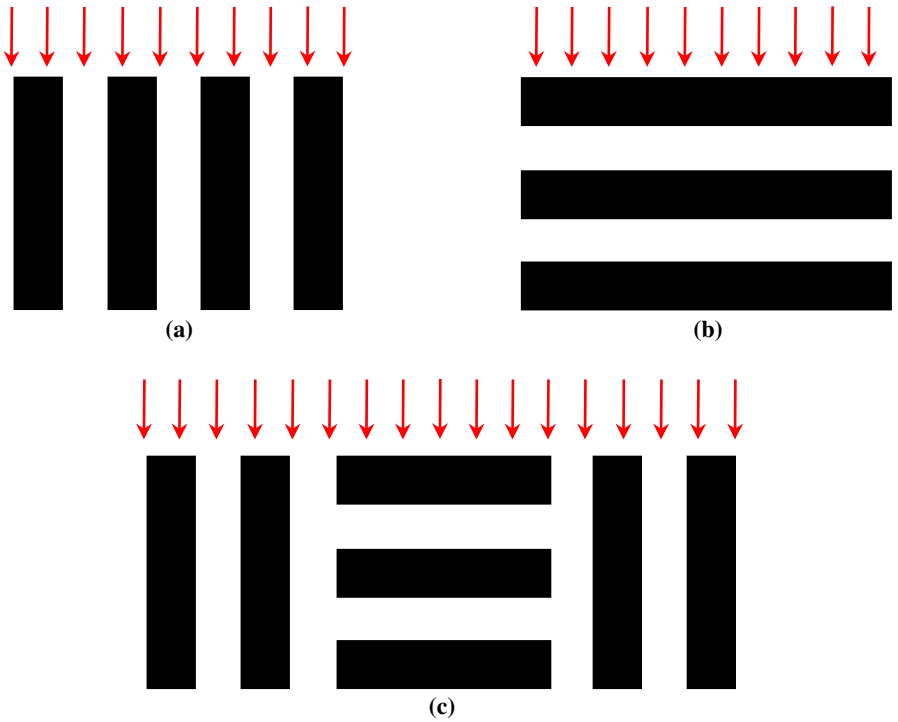

Fig. 10 Representations of the (a) parallel, (b) series and (c) parallel-series models for the structure of the distillation membranes. Black strips represent the solid matrix of the membrane whereas the white strips represent the void filled with the gaseous phase. The red arrows represent the direction of the heat flux.

Using the parameters used for the base case, Fig. 12 show how the KPIs change with α. It is clear that the model used to calculate the effective thermal conductivity has a significant effect on the KPI of the MD module: $\bar{J}$, η_t and TPC increase more than 55, 95 and 45% respectively when α decreases from 1 (parallel model) to zero (series model); this signifies the importance of selection of an appropriate model to estimate the effective thermal conductivity of the membrane. The effective thermal conductivity decreases with decreasing α, resulting in a decreased heat transfer through conduction between the feed and the permeate channels; an increased temperature difference and, subsequently, an increased difference in saturation

pressure of water vapour across the membrane; and ultimately improvement in all the KPIs of the MD module.

Nonetheless, further experimental investigations are required to accurately characterise the effective thermal conductivity of the commonly-used distillation membranes. The outcomes of such investigations will assist in identification the most appropriate model for each membrane or a set of membranes.

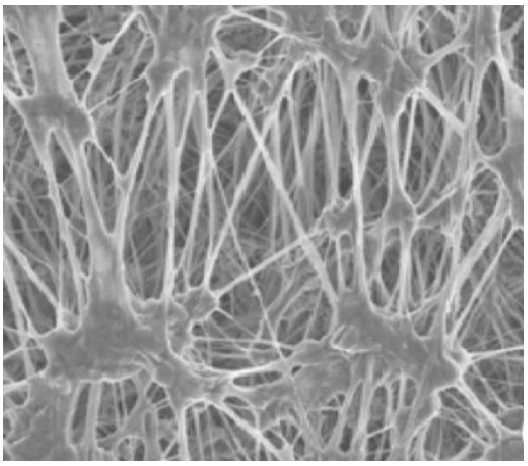

Fig. 11 An SEM image for a surface of a membrane. Reprinted from [13] with permission from Elsevier.

Table 5 Measured and calculated thermal conductivities for a number of membranes at ~ 25°C. Properties of the membranes were taken from [24]. The letters 'm' and 'c' stand for measured and calculated respectively.

Membrane	$k_{eff(m)}$ (W/m/K)	ε	k_s (W/m/K)	k_g (W/m/K)	Parallel		Series		Parallel-series	
					$k_{eff(c)}$ (W/m/K)	Error (%)	$k_{eff(c)}$ (W/m/K)	Error (%)	$k_{eff(c)}$ (W/m/K)	Error (%)
PVDF (Millipore)	0.041	0.62	0.17	0.02	0.077	87.80	0.030	26.61	0.039	3.73
PVDF (Millipore)	0.04	0.66	0.17	0.02	0.071	77.50	0.029	28.57	0.037	7.36
PTFE (Gore)	0.031	0.9	0.25	0.02	0.043	38.71	0.028	28.95	0.040	15.42
PTFE (Gore)	0.027	0.89	0.25	0.02	0.045	67.78	0.022	17.59	0.026	0.51

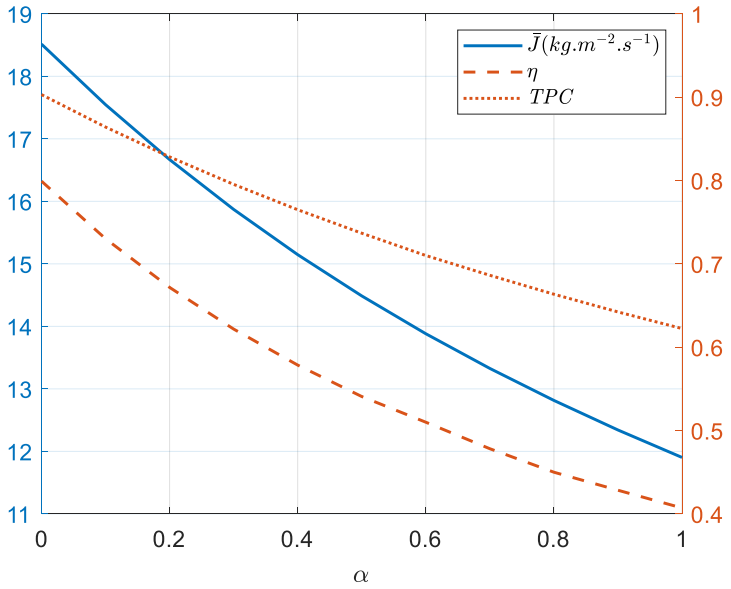

Fig. 12 The key performance indicators ($\bar{J}, \eta_t, TPC$) as a function of the weight factor α.

4. Conclusions and recommendations

A two-dimensional numerical model for a direct contact membrane distillation (DCMD) module has been developed. All the key physics that govern the transport of mass, momentum and energy have been incorporated into the model. Further, the spatial changes of the physical properties of the fluids flowing in the channels and the membrane with temperature have been taken into account. The model has been used to study the sensitivity of the key performance indictors or KPIs (i.e. the transmembrane flux ($\bar{J}$), the thermal efficiency (η_t) and the temperature polarisation coefficient (TPC)) to the operational conditions and the key characteristics of the membrane. Further, light has been shed on the existing models used to estimate the effective thermal conductivity of the membrane and a new model has been proposed. The following summarises the key findings of the study:

- Owing to the exponential relation between the saturation pressure of water vapour and temperature, the transmembrane flux is highly sensitive to the inlet temperature of the feed (hot) stream; for example $\bar{J}$, for the given conditions and parameters, increases more than fivefold if T_{hi} increases from ~ 40 to ~ 80 °C.
- The characteristics of the membrane, in particular its porosity (ε), have substantial impact on the KPIs of the MD module, especially with low inlet feed temperatures (e.g. ~ 40 °C). As ε increases, the effective diffusion coefficient increases and effective thermal conductivity decreases, thus decreasing the mass transport resistance and the heat transfer across the membrane and, ultimately, resulting in improved $\bar{J}$, η_t and TPC.
- As the thermal conductivity of the material of the membrane (k_s) increases, the gains in KPIs decrease. The increase in k_s leads to an increase in the effective thermal conductivity of the membrane and a subsequent increase in the conductive heat transfer through the

membrane, thus resulting in less temperature (and saturation pressure of water vapour) gradient across the membrane.

- As intuitively expected, $\bar{J}$ increases with increasing pore size (d_p), decreasing tortuosity (τ) and decreasing thickness (t_m) of the membrane.
- Theoretically, the salinity of the feed stream has, for the given range, almost negligible effect on all the KPIs.
- The thermal boundary layers decrease with increasing flow rates of the feed and the permeate streams (represented by $\boldsymbol{u}_{hi}$ and $\boldsymbol{u}_{ci}$), leading to an increased TPC and, subsequently, increased $\bar{J}$. On the other hand, η_t decreases with increasing $\boldsymbol{u}_{ci}$ and this is attributed to the decreased temperature difference across the membrane.
- At relatively high inlet feed temperature or T_{hi} (e.g. 80 °C), the inlet permeate temperature (T_{ci}) has a threshold value below which $\bar{J}$ increases with increasing T_{ci}; this is, unlike the situations with low (40 °C) or intermediate (60 °C) T_{hi}, due to the fact that the decrease in the temperature of the membrane-feed channel interface with increasing T_{ci} is so low to be outweighed by the increase in the temperature of the membrane-permeate channel interface.
- Likewise, the effect of the inlet permeate velocity or $\boldsymbol{u}_{ci}$ on $\bar{J}$ was shown to depend on the value of T_{hi}. As $\boldsymbol{u}_{ci}$ increases, $\bar{J}$ decreases with a relatively high inlet feed temperature (80 °C); the rate of decrease of the temperature of the membrane-feed channel interface, relative to those with 40 or 60 °C T_{hi}, increase with increasing $\boldsymbol{u}_{ci}$.
- The models used estimate the effective thermal conductivity of the membrane do not appear sufficiently accurate. The model that takes into account both the parallel and series configurations of the fibres has been proposed.

Based on the outcomes of the study, two key recommendations could be made:

- If the heat source that is used to heat up the feed stream of the MD module is not of financial concern (e.g. industrial waste heat), then it should be fully utilised to maximise the inlet temperature of the feed stream.
- Further experimentation is needed to accurately characterise the effective thermal conductivity (k_{eff}) of the membranes to assist in developing more accurate models for the estimation of k_{eff}.

Nomenclature

a	*Activity coefficient*
h_{fg}	*Heat of vaporisation (J kg^{-1})*
C_p	*Specific heat capacity (J mol^{-1} K^{-1})*
D_K	*Knudsen diffusion coefficient (m^2 s^{-1})*
D_w	*Normal (ordinary) diffusion coefficient (m^2 s^{-1})*
$\bar{J}$	*Average transmembrane flux (kg m^{-2} s^{-1})*
S_T	*Heat source term (W m^{-3})*
d_p	*Pore diameter of the membrane (m)*
p_s	*Saturation pressure (Pa)*
q_c	*Heat flux due to conduction (W m^{-2})*
q_l	*Heat flux due to latent heat (W m^{-2})*
t_m	*Membrane thickness (m)*
w_s	*Mass fraction of NaCl*
η_t	*Thermal efficiency*
C	*Molar concentration (mol m^{-3})*
L	*Length of the membrane distillation module (m)*
M	*Molecular weight (kg mol^{-1})*
N	*Transmembrane molar flux (mol m^{-2} s^{-1})*
R	*Universal gas constant (J mol^{-1} K^{-1})*
T	*Temperature (K)*
TPC	*Temperature polarisation coefficient*
k	*Thermal conductivity (W m^{-1} K^{-1})*
x	*Mole fraction*
$\boldsymbol{u}$	*Velocity vector (m s^{-1})*
α	*Weight factor*
ε	*Membrane porosity*
μ	*Dynamic viscosity (Pa s)*
ρ	*Density (kg m^{-3})*

τ	*Membrane tortuosity*

Subscripts

h	*Hot*
c	*Cold*
eff	*Effective*
f	*Feed*
g	*Gas*
i	*Inlet*
l	*Left*
mf	*Membrane-feed channel interface*
mp	*Membrane-permeate channel interface*
p	*Permeate*
r	*Right*
s	*Solid*
t	*Total*
w	*Water*

Acknowledgments

The authors would like to thank the Institutional Links Newton-Mosharafa Fund (261749278 and STIFA-27653) and Research England QR GCRF Institutional Allocation (X/165302) for their financial support.

Appendix A

The following temperature-dependent polynomials were used to estimate the density (ρ), dynamic viscosity (μ), specific heat capacity at constant pressure (C_p) and thermal conductivity (μ) of the flowing fluid in the feed and permeate channels (i.e. liquid water) [25]:

$$\rho = 838.466 + 1.401T - 3.011 \times 10^{-3}T^2 + 3.718 \times 10^{-7}T^3 \quad \text{(A.1)}$$

$$\mu = 1.38 - 2.122 \times 10^{-2}T + 1.360 \times 10^{-4}T^2 - 4.645 \times 10^{-7}T^3 + 8.904 \times 10^{-10}T^4 - 9.079 \times 10^{-13}T^5 + 3.846 \times 10^{-16}T^5 \quad \text{(A.2)}$$

$$C_p = 12010.1471 - 80.407T + 0.310T^2 - 5.382 \times 10^{-4}T^3 + 3.625 \times 10^{-7}T^4 \quad \text{(A.3)}$$

$$k = -0.869 + 8.949 \times 10^{-3}T - 1.584 \times 10^{-5}T^2 + 7.975 \times 10^{-9}T^3 \quad \text{(A.4)}$$

Appendix B

The changes of the KPIs with the investigated parameters with inlet feed temperatures of 40 and 80 °C are provided in Fig. A1 and Fig. A2 respectively.

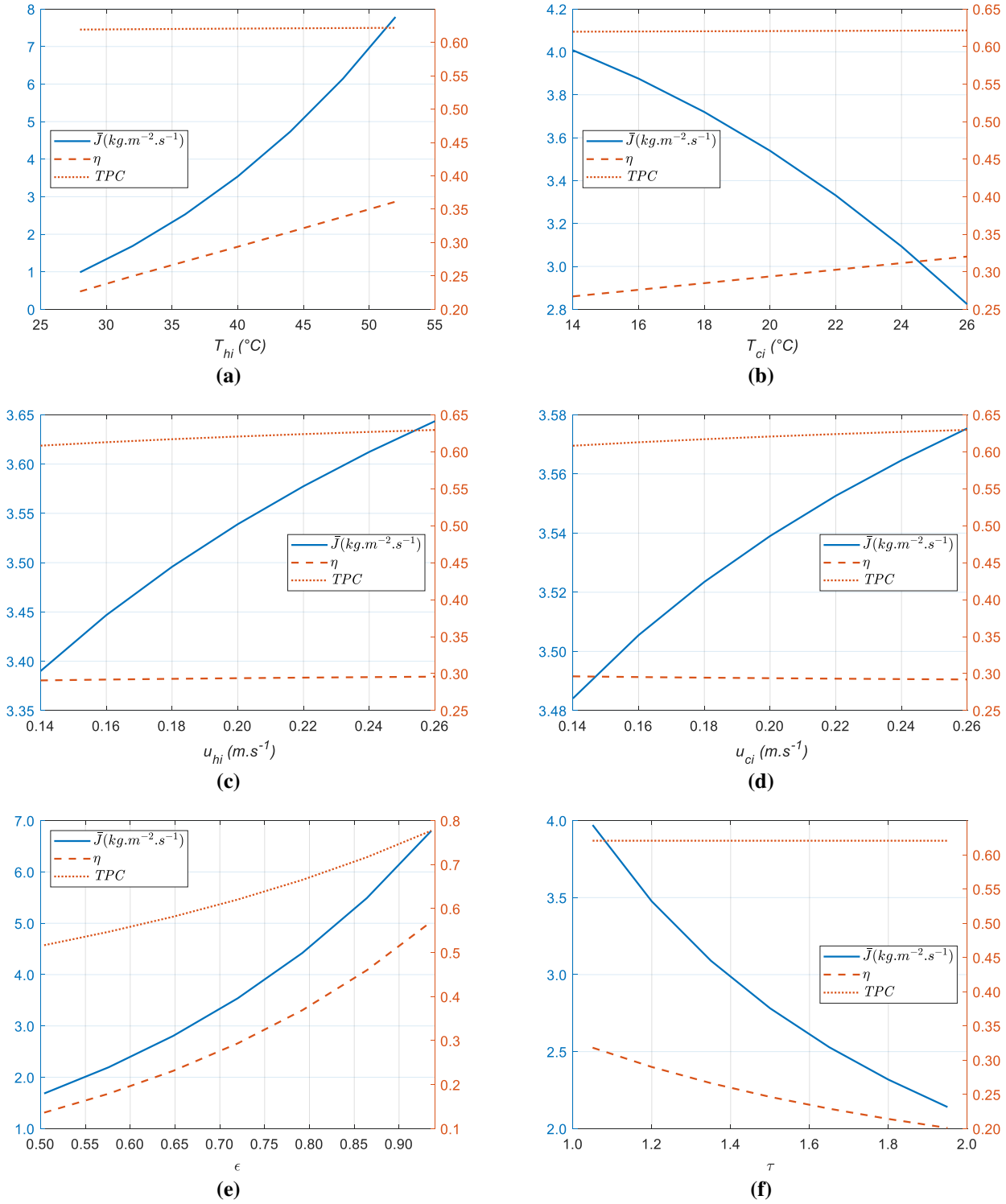

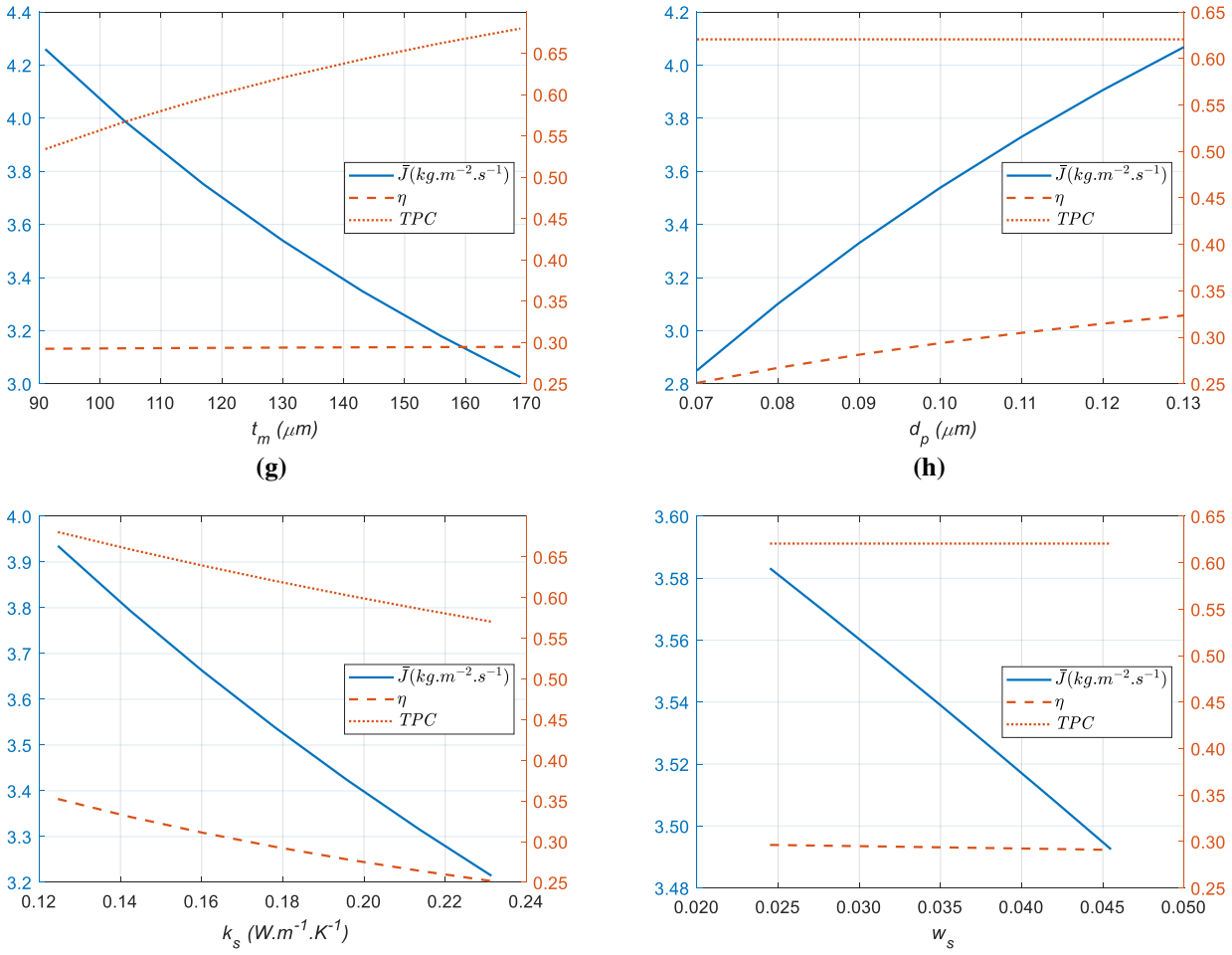

Fig. A1 The transmembrane flux ($\bar{J}$), thermal efficiency (η_t), and temperature polarisation coefficient (TPC) as functions of: (a) inlet feed temperatures (T_{hi}), (b) inlet permeate temperature (T_c), (c) inlet feed velocity (u_{hi}), (d) inlet permeate velocity (u_{ci}), (e) porosity (ε), (f) tortuosity (τ), (g) membrane thickness t_m, (h) average pore diameter (d_p), (i) thermal conductivity of the solid phase (k_s) and (j) salinity of water (w_s). The base inlet feed temperature is 40 °C.

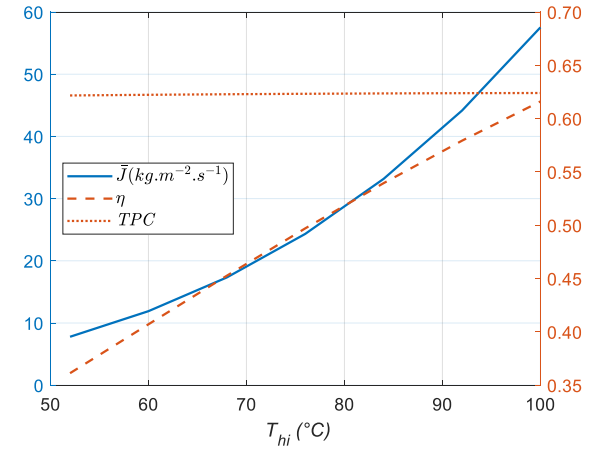
$\bar{J}(kg.m^{-2}.s^{-1})$
η
TPC
T_{hi} (°C)

(a)

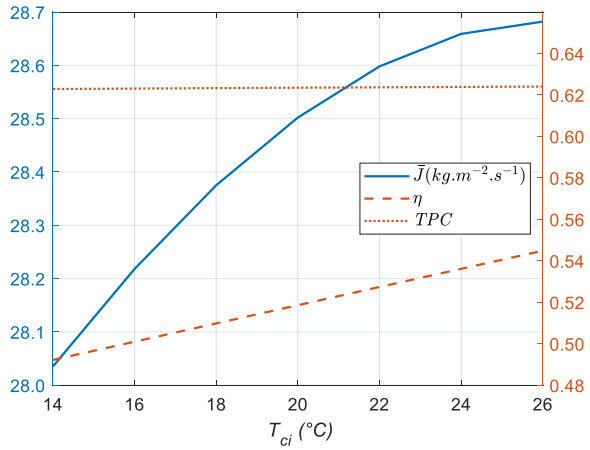
$\bar{J}(kg.m^{-2}.s^{-1})$
η
TPC
T_{ci} (°C)

(b)

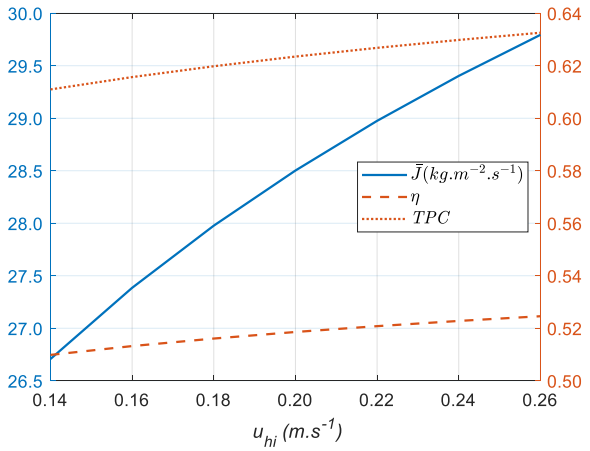
$\bar{J}(kg.m^{-2}.s^{-1})$
η
TPC
u_{hi} (m.s^{-1})

(c)

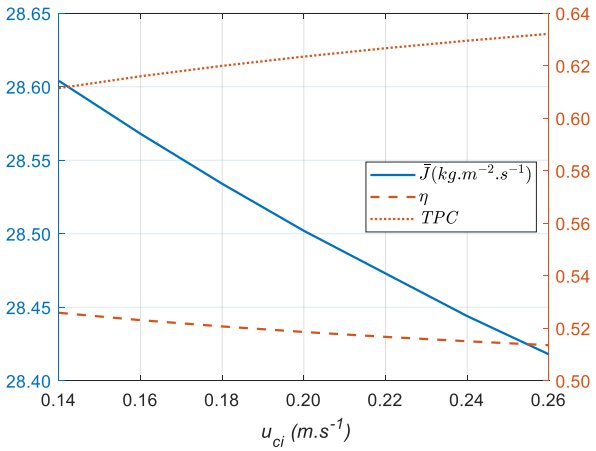
$\bar{J}(kg.m^{-2}.s^{-1})$
η
TPC
u_{ci} (m.s^{-1})

(d)

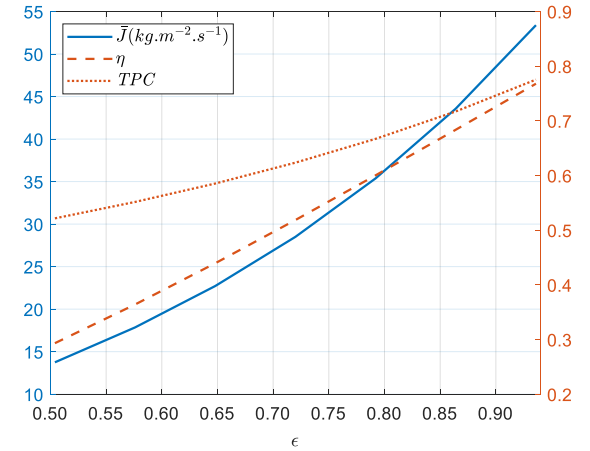
$\bar{J}(kg.m^{-2}.s^{-1})$
η
TPC
ϵ

(e)

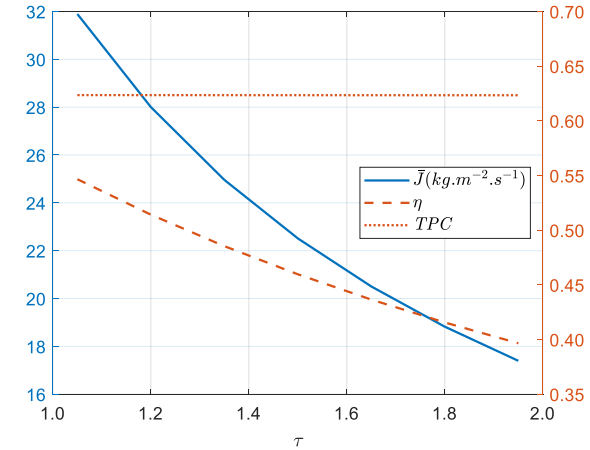
$\bar{J}(kg.m^{-2}.s^{-1})$
η
TPC
τ

(f)

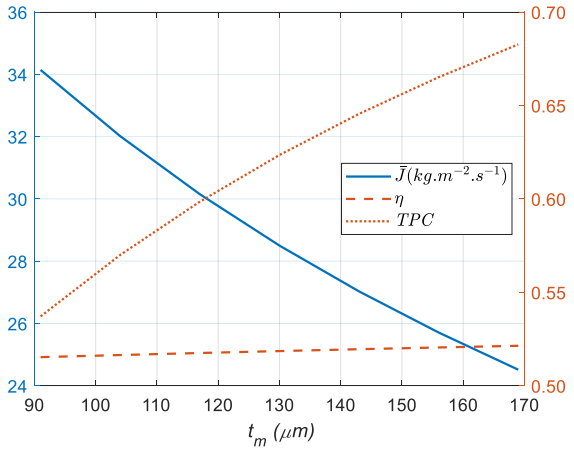

(g)

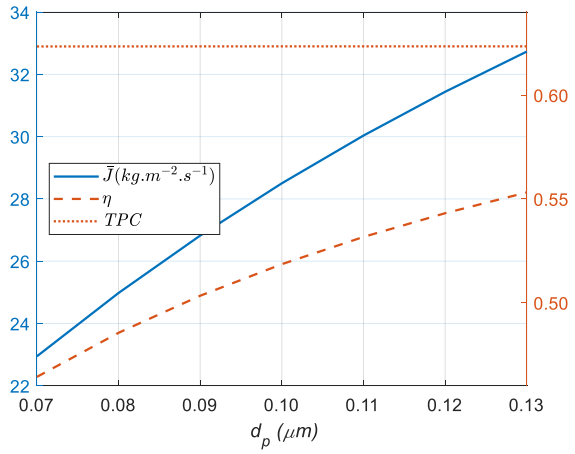

(h)

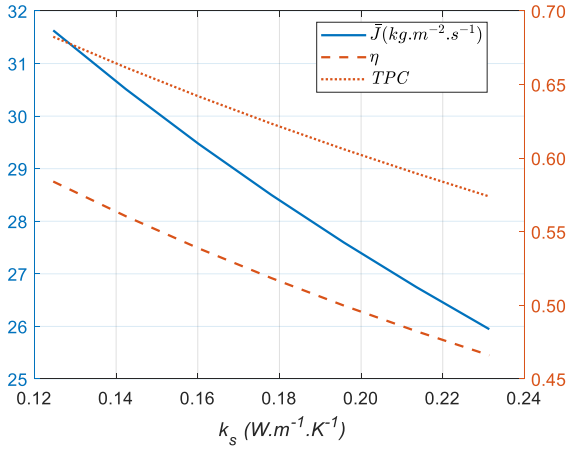

(i)

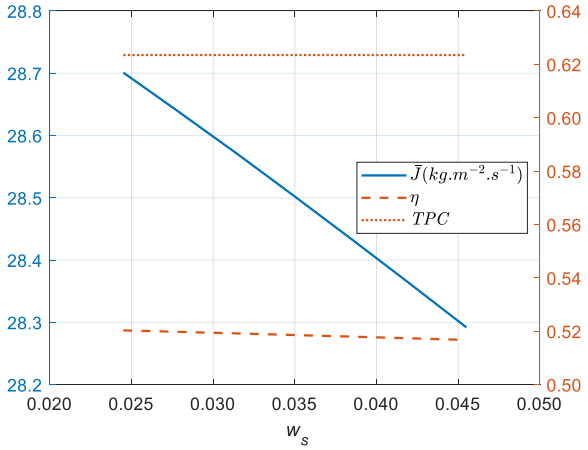

(j)

Fig. A2 The transmembrane flux ($\bar{J}$), thermal efficiency (η_t), and temperature polarisation coefficient (TPC) as functions of: (a) inlet feed temperatures (T_{hi}), (b) inlet permeate temperature (T_{ci}), (c) inlet feed velocity (u_{hi}), (d) inlet permeate velocity (u_{ci}), (e) porosity (ε), (f) tortuosity (τ), (g) membrane thickness t_m, (h) average pore diameter (d_p), (i) thermal conductivity of the solid phase (k_s) and (j) salinity of water (w_s). The inlet feed temperature is 80 °C.

1 # References

[1] D.J. Park, E. Norouzi, C. Park, Experimentally-validated computational simulation of direct contact membrane distillation performance, Int. J. Heat and Mass Trans. 129 (2019) 1031 – 1042.

[2] S. Lin, N.Y. Yip, M. Elimelech, Direct contact membrane distillation with heat recovery: Thermodynamic insights from module scale modeling, J. Membr. Sci. 453 (2014) 498 – 515.

[3] J. Zhang, N. Dow, M. Duke, E. Ostarcevic, J.D. Li, S. Gray, Identification of material and physical features of membrane distillation membranes for high performance desalination, J. Membr. Sci. 349 (2010) 295 – 303.

[4] A. Deshmukh, M. Elimelech, Understanding the impact of membrane properties and transport phenomena on the energetic performance of membrane distillation desalination, J. Membr. Sci. 539 (2017) 458 – 474.

[5] K.W. Lawson, D.R. Lloyd, Membrane distillation. II. Direct contact MD, J. Membr. Sci. 120 (1996) 123 – 133.

[6] A.M. Alklaibi, N Lior, Membrane-distillation: status and potential, Desalination 171 (2004) 111 – 131.

[7] Sarti, C. Gostoli, S. Bandini, Extraction of organic components from aqueous streams by vacuum membrane distillation, J. Membr. Sci. 80 (1993) 21 – 33.

[8] M.C. García-Payo, M.A. Izquierdo-Gil, C. Fernández-Pineda, Air gap membrane distillation of aqueous alcohol solutions, J. Membr. Sci. 169 (1) (2000) 61–80.

[9] M. Khayet, P. Godino, J. I. Mengual, Theory and experiments on sweeping gas membrane distillation, J. Membr. Sci. 165 (2000) 261-272

[10] M. Shakib, S.M.F. Hasani, I. Ahmed, R.M. Yunus, A CFD study on the effect of spacer orientation on temperature polarization in membrane distillation modules, Desalination 284 (2012) 332-340.

[11] H. Yu, X. Yang, R. Wang, A. Fane, Analysis of heat and mass transfer by CFD for performance enhancement in direct contact membrane distillation, J. Membr. Sci. 405-406 (2012) 38-47.

[12] T.C. Chen, C.D. Ho, H.M. Yeh, Theoretical modeling and experimental analysis of direct contact membrane distillation, J. Membr. Sci. 330 (2009) 279-287.

[13] H.J. Hwang, K. He, S. Gray, J. Zhang, I.S. Moon, Direct contact membrane distillation (DCMD): Experimental study on the commercial PTFE membrane and modeling, J. Membr. Sci. 371 (2011) 90-98.

[14] A.M. Alklaibi, N. Lior, Comparative Study of Direct-Contact and Air-Gap Membrane Distillation Processes, Ind. Eng. Chem. Res. 46 (2007) 584-590.

[15] I. Janajreh, D. Suwwan, R. Hashaikeh, Assessment of direct contact membrane distillation under different configurations, velocities and membrane properties, App. Energy 185 (2017) 2058-2073.

[16] V. Perfilov, A. Ali, V. Fila , A general predictive model for direct contact membrane distillation, Desalination 445 (2018) 181 – 196.

[17] H. Hayer, O. Bakhtiari, T. Mohammadi, Simulation of momentum, heat and mass transfer in direct contact membrane distillation: A computational fluid dynamics approach, J. Ind. Eng. Chem. 21 (2015) 1379 – 1382.

[18] M. Rezakazemi, CFD simulation of seawater purification using direct contact membrane desalination (DCMD) system, Desalination 443 (2018) 323-332.

[19] T.L. Bergman, A.S. Lavine, F.P. Incropera, D.P. Dewitt, Fundamentals of Heat and Mass Transfer, 7th edition, 2011, John Wiley & Sons, US.

[20] K.W. Lawson, D.R. Lloyd, Membrane distillation, J. Membr. Sci. 124 (1997) 1-25.

[21] A. Alkhudhiri, N. Darwish, N. Hilal, Membrane distillation: A comprehensive review, Desalination 287 (2012) 2-18.

[22] J. Phattaranawik, R. Jiraratananon, A.G. Fane, Effect of pore size distribution and air flux on mass transport in direct contact membrane distillation, J. Membr. Sci. 215 (2003) 75-85.

[23] S. Soukane, M.W. Naceur, L. Francis, A. Alsaadi, N. Ghaffour, Effect of feed flow pattern on the distribution of permeate fluxes in desalination by direct contact membrane distillation, Desalination 418 (2017) 43-59.

[24] J. Phattaranawik, R. Jiraratananon, A.G. Fane, Heat transport and membrane distillation coefficients in direct contact membrane distillation, J. Membr. Sci. 212 (2003) 177-193.

[25] Material Library. COMSOL Multiphysics® v. 5.2. COMSOL AB, Stockholm, Sweden. 2020